Hindawi
Journal of Nanomaterials
Volume 2019, Article ID 6854710, 10 pages
https://doi.org/10.1155/2019/6854710

Research Article

Biological Characteristics and Carrier Functions of Pegylated Manganese Zinc Ferrite Nanoparticles

Ting Guo[1], **Fengxiao Dou**[2], **Mei Lin**[3], **Junxing Huang**[4], **Chenglin Zhou**[3], **Jun Zhang**[5], **Hong Yu**[6], **Xingmao Jiang**[7], **Jun Ye**[1], **Yujuan Shi**[1], **Yanhong Xiao**[1], **Xuefeng Bian**[1], **Xiaoqian Feng**[1] **and Ning Xu**[8]

[1]*Institute of Clinical Medicine, Taizhou People's Hospital Affiliated to Nantong University, Taizhou, Jiangsu 225300, China*
[2]*Medical Image Center, Taizhou People's Hospital Affiliated to Nantong University, Taizhou, Jiangsu 225300, China*
[3]*Clinical Laboratory, Taizhou People's Hospital Affiliated to Nantong University, Taizhou, Jiangsu 225300, China*
[4]*Oncology Department, Taizhou People's Hospital Affiliated to Nantong University, Taizhou, Jiangsu 225300, China*
[5]*Department of Nuclear Medicine, Taizhou People's Hospital Affiliated to Nantong University, Taizhou, Jiangsu 225300, China*
[6]*Pathology Department, Taizhou People's Hospital Affiliated to Nantong University, Taizhou, Jiangsu 225300, China*
[7]*Hubei Key Lab of Novel Reactor & Green Chemical Technology, Key Laboratory for Green Chemical Process of Ministry of Education, School of Chemical Engineering and Pharmacy, Wuhan Institute of Technology, Wuhan 430205, China*
[8]*Gastrointestinal Surgery, Taizhou People's Hospital Affiliated to Nantong University, Taizhou, Jiangsu 225300, China*

Correspondence should be addressed to Mei Lin; l_mei@163.com

Ting Guo and Fengxiao Dou contributed equally to this work.

Received 24 July 2019; Accepted 23 October 2019; Published 18 November 2019

Academic Editor: Ruibing Wang

This study was performed to investigate the biocompatibility (BC), magnetothermal effect, and DNA binding biological characteristics of manganese zinc ferrite nanoparticles ($Mn_{0.6}Zn_{0.4}Fe_2O_4$-NPs (MZF-NPs)) coated with pegylated manganese (PEG-MZF-NPs). Their functions as gene transfer carrier for gene therapy and magnetic medium for tumor hyperthermia were also explored. The manganese zinc ferrite nanoparticles were synthesized through high temperature cracking, and their characterizations were discovered. Hemolysis test and MTT assay were performed to evaluate biocompatibility, and their self-heating effects in the alternating magnetic field were investigated. PEG-MZF-NPs with different concentrations were measured by using 7.0 T Micro-MR scanner (MRI) to calculate the T2 value and r2 relaxation rate of each sample. The CD44-shRNA plasmids were constructed, and their ability to bind PEG-MZF-NPs were examined. The DNA release from PEG-MZF-NP/DNA complex and protection of DNA from nuclease digestion were also detected. After CD44-shRNA-EGFP were transfected into the ovarian cancer SK-OV-3 cells by using PEG-MZF-NPs as carriers, the transfection efficiency was detected by a flow cytometer and expression of CD44 mRNA and protein in cells was detected using RT-PCR and Western blot, respectively. We successfully prepared PEG-MZF-NPs with favorable dispersity, magnetic responsiveness, and BC. Typically, the excellent magnetothermal effect can be used for a tumor magnetothermal therapeutic study. *In vitro* MRI showed the application potential for being magnetic resonance T2 relaxation contrast agents and the possibility to achieve goal of integration of targeting diagnosis and treatment. The CD44-shRNA plasmids have been successfully constructed and concluded that PEG-MZF-NPs may serve as gene transfer carriers for gene therapy.

1. Introduction

With the development of nanotechnology, nanoparticles (NPs) used as gene and drug carrier have been extensively studied [1, 2]. Owing to some special properties such as easy modifiability, good biocompatibility, little immune response, and being easily coupled with other ligands and easily organized with specific cell surface receptors or swallowed up by target cells and high efficiency rate gene transfer, nanoparticles can be made as ideal carriers [3]. Apart from the general functions of a nanocarrier, magnetic nanoparticles can produce a thermal effect in an alternating magnetic field and hence may be used for tumor hyperthermia [4, 5].

Magnetic iron oxide (Fe3O4, Fe2O3) nanoparticles are widely used metallic oxides. The doping of metal elements such as manganese and zinc in a nanosized iron oxide structure can compose a variety of ferrites. Among them, manganese zinc ferrite ($Mn_{0.6}Zn_{0.4}Fe_2O_4$, $Mn_{0.5}Zn_{0.5}Fe_2O_4$) nanoparticles have been used as vectors in suicide gene HSV-TK therapy for hepatoma and showed a satisfactory effect [6]. Moreover, manganese zinc ferrite nanoparticles also possess automatic temperature control and homoeothermic features [4, 7]. It is considered that manganese zinc ferrite nanoparticles may be used as a vehicle for CD44-shRNA therapy and function as a magnetic medium for magnetic thermotherapy on ovarian cancer.

In the current study, $Mn_{0.6}Zn_{0.4}Fe_2O_4$ nanoparticles (MZF-NPs) were synthesized by high temperature cracking and then surface-modified with polyethylene glycol (PEG) and CD44-shRNA plasmids were constructed. The biocompatibility (BC) of PEG-MZF-NPs was investigated by a hemolysis test and MTT assay. The feasibility of PEG-MZF-NPs used for CD44-shRNA carrier was explored, and the magnetothermal effect of CD44-shRNA/PEG-MZF-NPs was examined.

2. Materials and Methods

2.1. PEG-MZF-NP Preparation and Characterization. The spherical magnetic manganese zinc ferrite nanoparticles wrapped with oleic acid were prepared using a high-temperature cracking method, and then PEG2000 (Sangon, China) was used to coat MZF-NPs. In brief, PEG2000 dissolved in chloroform was mixed with MZF-NPs followed by ultrasonic dispersion for 10 min. Subsequently, deionized water was added. The resultant was placed on a rotary evaporator for vacuum suction at 70°C to prepare PEG-MZF-NPs [7]. A small number of PEG-MZF-NPs were dissolved in the absolute ethanol followed by 20 min of ultrasonic dispersion and then dripped onto an encapsulated copper wire mesh to prepare high-resolution transmission electron microscope (TEM, TecnaiG20, FEI, USA) samples. Finally, the sample's morphology was observed under a TEM. The magnetic response of PEG-MZF-NPs was measured by a vibration sample magnetometer at normal temperature within a magnetic field range of -100000*e* +100000*e*. The characteristic peak of PEG-MZF-NPs was analyzed by a Fourier transform microscopic infrared spectrometer (HYPERION, Bruker, Germany).

2.2. Heating Experiment In Vitro. PEG-MZF-NP magnetic fluids at the concentrations of 20 μg/mL, 40 μg/mL, 60 μg/mL, and 80 μg/mL were prepared. The temperature was recorded every 5 min from high-frequency magnetic induction heating equipment (Shuangping Power, Shenzhen, China) in an alternating magnetic field (235 kHz, 4 kW, and 35 A). Afterwards, the heating curve was plotted with temperature as a vertical coordinate and time as a horizontal coordinate.

2.3. Cell Culture. Ovarian cancer SK-OV-3 cells and mouse fibroblast L929 cells were purchased from the Cell Bank of Chinese Academy of Sciences (Shanghai, China). SK-OV-3 cells and L929 cells were cultured in an IMDM medium (GIBCO, Thermo Fisher Scientific, America) containing 10% FBS (Evergreen, China) at a constant temperature of 37°C and a constant humidity of 5% CO_2.

2.4. Cytotoxicity Experiment. L929 cells at a logarithmic phase were divided into 5 groups at the cell counting concentration of 5×10^4/mL which include the negative control group, PEG-MZF-NP groups (at the concentrations of 40 μg/mL, 60 μg/mL, and 80 μg/mL), and positive control group (0.7% acrylamide solution). Six duplicate wells were set for each group. Cells were inoculated into the 96-well plates to incubate for 24 h, and 20 μL MTT (Sangon, China) solution (5 mg/mL) was then added into each well. After incubation in the saturated humidity incubator at 37°C and 5% CO_2 for 4 h, the original solution was discarded. Then 150 μL DMSO (MPBIO, America) was added into each well followed by oscillation for 10 min on a microplate reader (Huarui, China), and the optical density (OD) value was read at wavelength of 500 nm. The cell proliferation rate (RGR%) = (OD value in experiment group/OD value in control group) × 100%.

2.5. Hemolysis Test. The fresh normal saline for anticoagulation was diluted at a ratio of 1 : 2. PEG-MZF-NPs were dissolved in 10 mL normal saline (final concentration of 60 μg/mL). The 10 mL normal saline was used as the negative control and 10 mL distilled water was used as the positive control, and 3 parallel tubes were set for each group. 0.2 mL diluted anticoagulated normal saline was added into each group followed by a water bath for 1 h at 37°C and centrifugation for 5 min at 3500 r/min. The OD value in each group was read using a microplate reader at a wavelength of 545 nm. Hemolysis rate (%) = (the mean OD value of the tested sample − the mean OD value of the negative control group)/(the mean OD value in the positive control group − the mean OD value in the negative control group) × 100. A hemolysis rate of <5% indicated that such material had no hemolysis effect.

2.6. MRI Study of PEG-MZF-NPs In Vitro. PEG-MZF-NPs with a concentration of 0.04, 0.08, 0.16, 0.32, 0.64, and 1.28 g/mL were placed in an Eppendorf tube containing 1% agarose. The control group was agarose with deionized water. A 7.0 T microMR scanner (Bruker, Germany), a body coil with an inner diameter of 3.0 cm, and an SE T2W1 sequence were used. The parameters were set as follows: repeat time

2500 ms, echo time 36 ms, layer thickness 1.0 mm for 4 cm × 3.5 cm, and matrix 256 by 256. The corresponding T2 values of each sample were read, and then r2 curve (r2 = 1/T2) was made under origin to obtain a relaxation rate of r2 of each concentration sample.

2.7. Construction of the CD44-shRNA Eukaryotic Expression Plasmid. The CD44v6-shRNA primer sequences were purchased from Suzhou Jinweizhi Company. The CD44v6 primer sequence upstream was 5′-GATCCCCGGCAACT CCTAGTAGTACATTCAAGAGATGTACTACTAGGAGTT GCCTTTTTA-3′, and the downstream was 5′-AGCTTAAAA AGGCAACTCCTAGTAGTACATCTCTTGAATGTACTAC TAGGAGTTGCCGGG-3′. The primers were annealed, the shRNA segment was prepared, and the enzyme digestion carrier was also prepared followed by connection, transformation, plate coating, and sequencing after shaking bacterial solution. The reaction conditions of CD44-shRNA were as follows: initial denaturation at 95°C for 5 min; 30 cycles of 94°C for 30 s, 60°C for 30 s, and extension at 72°C for 30 s, followed by the final extension at 72°C for 10 min. Meanwhile, CD44-shRNA-EGFP plasmids were also constructed for transfection efficiency detection.

2.8. PEG-MZF-NPs Binding with CD44-shRNA Experiment. PEG-MZF-NPs were mixed with CD44-shRNA plasmids at the mass ratios of 0 : 1, 5 : 1, 10 : 1, 20 : 1, 40 : 1, and 80 : 1 at normal temperature for 30 min, and then 5 μL of each complex was taken for agarose gel electrophoresis (AGE) to screen the optimal binding ratio.

2.9. DNA Digestion Protection Capacity. Tango Buffer and DNase-I enzyme (Solarbio, China) were added into the complex of PEG-MZF-NPs and CD44-shRNA plasmids at their mass ratio of 40 : 1 to digest for 1 min, 10 min, 30 min, 45 min, and 1 h. Subsequently, 100 mmol/L EDTA solution was added to terminate the reaction. The resultants were washed, dried, and dissolved in an appropriate amount of ultrapure water. An equivalent volume of each product was taken for AGE detection.

2.10. DNA Release Capacity of the Complex. The complex (PEG-MZF-NPs and CD44-shRNA plasmids at their mass ratio of 40 : 1 and 10 μg CD44-shRNA plasmids) was mixed with TE solution to 500 μL. Subsequently, 8 μL sample was taken at 1, 4, 8, 12, 24, 48, 72, and 96 h for AGE.

2.11. PEG-MZF-NP Transfection Efficiency Detection. PEG-MZF-NPs and CD44-shRNA-EGFP were dispersed in IMDM culture solution. After being incubated for 30 min, they were sufficiently mixed at the mass ratio 40 : 1 of PEG-MZF-NPs and CD44-shRNA-EGFP. After ovarian cancer SK-OV-3 cells were cultured for 24 h, this solution was replaced with the above mixture. After being incubated for 6 h, the solution was replaced by fresh IMDM and continued incubating for another 24 h before cells were harvested. In the meantime, a liposome (Solarbio, China) transfection method was also conducted in accordance with the kit instruction for comparison. The cell transfection efficiency of the two methods was analyzed using a flow cytometer (BD, America).

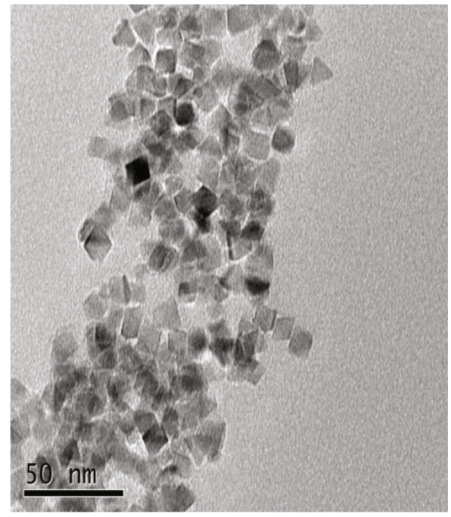

Figure 1: TEM images of PEG-MZF-NPs. The uniform of PEG-MZF-NPs in size had good dispersity examined by a transmission electron microscope (TEM) with their average particle size of about 10 nm.

2.12. CD44 mRNA and Protein Expression in Cells. Using PEG-MZF-NPs as carriers, CD44-shRNA plasmids and the empty plasmids were transfected into ovarian cancer SK-OV-3 cells. The mRNA and protein in cells were detected 24 h later by RT-PCR and Western Blot. The PCR primer sequences of CD44 (Beyotime, China) were as follows: upstream 5-GGCACCCGCTATGTCCAGAA-3 and downstream 5-CCTCCTGAAGTGCTGCTCCT-3; the internal reference gene GAPDH sequences (Beyotime, China) were as follows: upstream 5-CATCTTCTTTTGCGTCGCCA-3 and downstream 5-TTAAAAGCAGCCCTGGTGACC-3.

3. Results and Discussion

3.1. PEG-MZF-NP Preparation and Characterization. The unique properties of nanomaterials allow for their extensive application in biomedical field [8, 9]. As a type of nanomaterial, magnetic nanoparticles not only possess the physicochemical properties of general nanomaterials but also have magnetism and magnetothermal properties [10]. However, their highly absorptive property makes them extremely unstable. They tend to aggregate easily, bounding their equal distribution in media and thus limiting their application. Therefore, there is a need for their surface modification to improve their stability and biological functions. PEG is one of surface modifiers for magnetic NPs for injection *in vivo* [11]. It can bind onto the magnetic NP surface and can bind with other biological segments such as extremely unstable DNA segment outside cell or can bind with some types of drugs [8]. In the present study, when manganese zinc ferrite nanoparticles were modified with PEG, they had favorable water solubility and biocompatibility, which could be used as a gene or drug carrier. PEG-MZF-NPs examined by

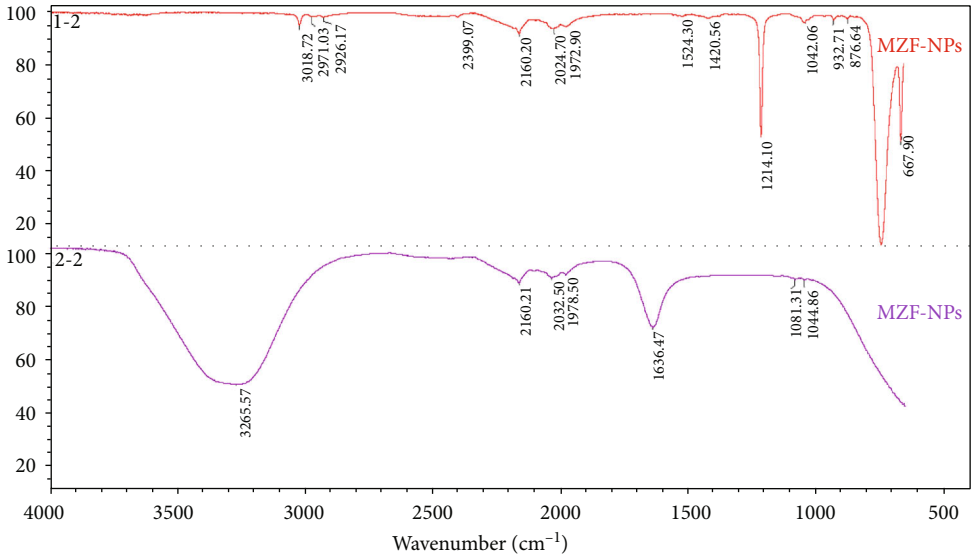

Figure 2: Fourier transform infrared spectroscopy (FTIR) of PEG-MZF-NPs. FTIR analysis of PEG-MZF-NPs with obvious PEG characteristic peaks at 3265 cm^{-1}, 1636 cm^{-1}, 1081 cm^{-1}, and 1044 cm^{-1}. These characteristic peaks were generated by O-H stretching vibration of PEG and C-H bending vibration.

TEM were about 10 nm, uniform in size, with good dispersity (Figure 1). PEG-MZF-NP magnetic fluid was a dark brown liquid with saturation magnetization of about 300 K and 98 emu/g. It had strong magnetic responsiveness, which increased with the increase of external magnetic field intensity. Figure 2 shows the FTIR analysis of PEG-MZF-NPs with obvious PEG characteristic peaks at 3265 cm^{-1}, 1636 cm^{-1}, 1081 cm^{-1}, and 1044 cm^{-1}. These characteristic peaks were generated by O-H stretching vibration of PEG and C-H bending vibration.

3.2. Heating Experiment In Vitro. In our previous study [4, 7], we prepared nanosized temperature-sensitive manganese zinc ferrite (Mn_xZn_1-xFe_2O_4) which had specific Curie temperature by adjusting the amount of Mn and Zn. The manganese zinc ferrite possessed magnetism at low temperature than Curie temperature. This magnetism could absorb the electromagnetic waves under action of alternating magnetic fields resulting in an increase in temperature. When reaching Curie temperature (such as 42-44°C), Mn_xZn_1-xFe_2O_4 becomes a nonmagnetic substance and losses its ability to absorb electromagnetic waves, resulting in a decrease in temperature. After the temperature falls below the Curie temperature, manganese zinc ferrite begins magnetic heating again. So cyclically, the temperature was always maintained around the Curie temperature. 42-44°C is an effective therapeutic temperature range for tumor which can kill tumor cells and destroy tumor tissue with few or no damage to normal tissues [12]. Thus, the difficulty of automatic temperature measurement and control in tumor hyperthermia was successfully solved, and the stability and safety of hyperthermia were improved. In current study, the heating experimental results *in vitro* are shown in Figure 3. In the applied high-frequency alternating magnetic field conditions (235 kHz, 4 kW, and 35 A), PEG-MZF-NPs could rapidly warm at various concentrations. The temperature sharply increased within the first 20 min, then slowly increased and maintained at a certain constant temperature during 20-50 min. The temperature of PEG-MZF-NPs at a concentration of 60 μg/mL was elevated to 42-44°C within 20 min. This is a desired temperature for tumor hyperthermia, suggesting PEG-MZF-NPs may serve as a magnetic mediator for tumor magnetic hyperthermia.

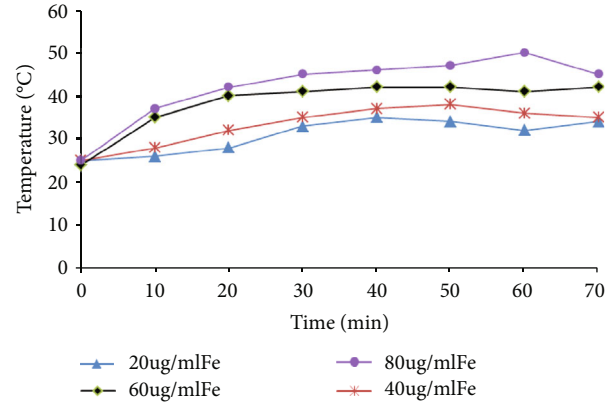

Figure 3: The magnetic induction heating curves of PEG-MZF-NPs at different concentrations *in vitro*. PEG-MZF-NPs at various concentrations could rapidly warm. The temperature sharply increased within the first 20 min, then slowly increased and maintained at a certain constant temperature during 20-50 min. The temperature of PEG-MZF-NPs at the concentration of 60 μg/mL was elevated to 42-44°C within 20 min which is an ideal desired temperature for tumor hyperthermia.

3.3. Cytotoxicity Detection. Cytotoxicity and hemolysis rate both are important indices to evaluate the biosafety of biomedical materials. MTT assay is a common method for

Table 1: MTT assay results after intervening L929 cells with PEG-MZF-NPs (mean ± s, $n = 4$).

Group	Absorbent biological material (OD value)	RGR (%)	Toxicity grade
Negative control group (MEM culture solution)	1.68 ± 0.13	100	0
40 μg/mL group	1.55 ± 0.11	93 ± 12	1
60 μg/mL group	1.45 ± 0.09	87 ± 10	1
80 μg/mL group	1.50 ± 0.09	89 ± 4	1
Positive control group (acrylamide solution)	0.60 ± 0.04	36 ± 3	5

MTT assay was employed to detect the toxicity of magnetic NPs at different concentrations. After PEG-MZF-NPs were cocultured with L929 cells, the cell proliferation rates of negative control group were all 100% or so, and the cytotoxicity was grade 0, suggesting no cytotoxicity. The magnetic NP group with concentrations ranging from 40 g/mL to 80 g/mL had grade 1 cytotoxicity. In comparison, the cell proliferation rate in the positive control group was 39% and the cytotoxicity was grade 5.

Table 2: OD value and hemolysis rate of material in each group (mean ± s, $n = 4$).

Group	Optical density (OD)	Hemolysis rate (%)
Negative control group	0.023 ± 0.006	0
Positive control group	0.603 ± 0.001	100%
PEG-MZF-NP group	0.030 ± 0.002	1.12%

According to the hemolysis test results, hemolysis rates of three groups were compared according to SPSS analysis of variance results ($P < 0.05$). The hemolysis rate of PEG-MZF-NP group was 1.12% (<5%) which meets the application standard of medical biological material (ISO10993).

detecting cytotoxicity. It is simple to perform with a good repeatability. In this study, MTT assay was employed to detect the toxicity of magnetic NPs at different concentrations and results are depicted in Table 1. It is clear that coculture of PEG-MZF-NPs with L929 cells resulted in about 100% cell proliferation rates with zero cytotoxicity. In comparison, the cell proliferation rate in the positive control group was 39% with grade 5 cytotoxicity indicating positive control was not an eligible medical material. The hemolysis rates of three groups were compared according to the SPSS analysis of variance results ($P < 0.05$). The hemolysis rate of the PEG-MZF-NP group was 1.12% (<5%) (Table 2) which meets the application standard of medical biological materials (ISO10993).

3.4. MRI Study of PEG-MZF-NPs In Vitro. In order to improve the sensitivity of MRI, contrast agents are often needed to improve the contrast and image quality in clinical applications. With the research and development of nanotechnology, nanomaterials have displayed broad application prospects in early detection of tumors and other diseases. PEG-MZF-NPs selected in this study have good stability and magnetic characteristics. Doped manganese and zinc metal elements can increase the magnetic properties of Fe_3O_4 and can be used as a high-performance MRI contrast agent [13]. In order to explore whether PEG-MZF-NPs can be used as an MRI contrast agent, PEG-MZF-NPs at different concentrations were scanned by MRI T2W1 sequence in the present study. As shown in the T2W1 image, T2W1 signal significantly decreased along with the concentration increase (Figure 4(a)). T2 values of PEG-MZF-NPs at different concentrations were measured, and the relaxation rate r2 of materials was 6.06 $\mu g \cdot mL^{-1}\ s^{-1}$ (Figure 4(b)). These findings indicate a good potential for the MRI contrast agent.

3.5. Construction and Identification of CD44-shRNA Eukaryotic Expression Plasmid. The 5 μL PCR product was taken for electrophoresis, and results are shown in Figure 5(a). The sequencing results suggested that after insertion of CD44-v6-shRNA gene segment, the positive clones were selected for PCR amplification. The bacterial solution was shaken, and the sequencing comparison confirmed that there were correct clones indicating successful construction of the CD44-v6-shRNA plasmid (Figure 5).

3.6. Binding, Digestion, and Release of PEG-MZF-NPs with CD44-shRNA. A gene carrier should have good tissue compatibility along with the ability to protect the gene segment from being degraded during transportation and can be effectively released after reaching the target cell. The electrophoresis images of binding, release, and digestion protection experiments suggested that clear bands could be seen in lanes when plasmids were added at ratios of 0 : 1, 5 : 1, 10 : 1, 20: 1, and 40 : 1. When the mass ratio of magnetic NPs to CD44-shRNA was 40 : 1, the former could practically bind with all plasmids in the system (Figure 6(a)) indicating 40 : 1 was an optimal binding ratio. Within 1, 4, 8, 12, and 24 h and 2 d, DNA was released at a large amount. But it was not greatly different between day 3 and day 4, and PEG-MZF-NPs could protect the plasmids and effectively release DNA (Figure 6(b)). In the stability research, a DNase-I digestion experiment was used to observe stability of magnetic nanomaterial/gene complex. The band lightness of PEG-MZF-NP/CD44-shRNA complex in the electrophoresis image showed no obvious changes within the first 60 min demonstrating its stability. The exposed CD44-shRNA plasmids were almost digested by DNase-I within 1 min suggesting a good stability of complex, and PEG-MZF-NPs could protect CD44-shRNA from nuclease digestion (Figure 6(c)).

3.7. Evaluation of PEG-MZF-NP Gene Transfection Efficiency. Gene therapy is a strategy by transferring exogenous genes or gene segments into target cells to intervene the target gene. However, DNA is extremely unstable and easily degraded by nucleotidase outside the cell. Therefore,

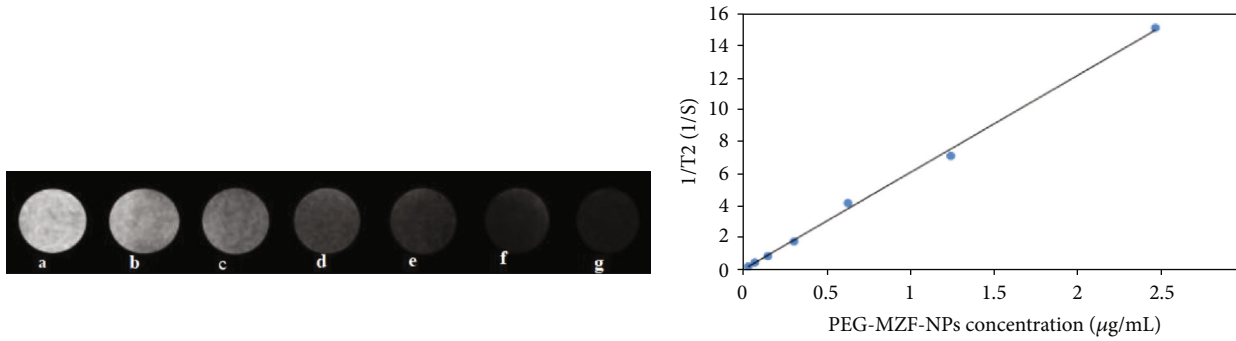

(a) (b)

Figure 4: MRI study of PEG-MZF-NPs *in vitro*. (a). MRI of magnetic PEG-MZF-NP with different concentrations *in vitro*: (A) a normal saline group; (B) 0.04 μg/mL PEG-MZF-NP group; (C) 0.08 μg/mL PEG-MZF-NP group; (D) 0.16 μg/mL PEG-MZF-NP group; (E) 0.32 μg/mL PEG-MZF-NP group; (F) 0.64 μg/mL PEG-MZF-NP group; (G) 1.28 μg/mL PEG-MZF-NP group. PEG-MZF-NPs with different concentrations were scanned for MRI T2W1 sequence. It can be observed from the T2W1 image that with an increase in material concentration, the T2W1 signal significantly decreased. (b) T2 transverse relaxation time of PEG-MZF-NPs at different concentrations (r2). T2 values of PEG-MZF-NPs at different concentrations were measured, and relaxation rate r2 of materials was 6.06 $\mu g \cdot mL^{-1}\ s^{-1}$. These findings indicate a good potential for the MRI contrast agent.

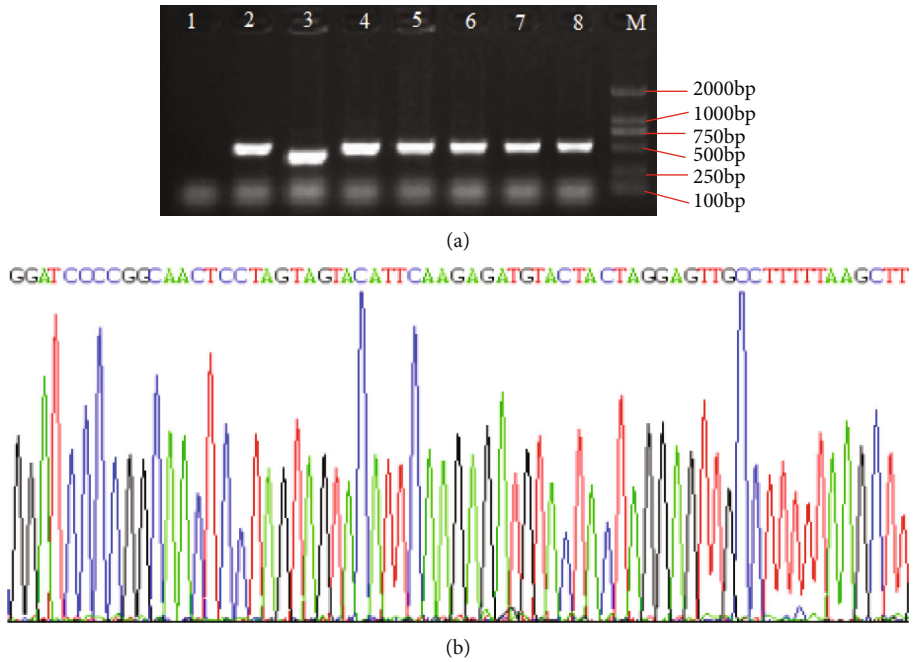

(a)

(b)

Figure 5: Construction and identification of CD44-shRNA eukaryotic expression plasmid. (a) Eletrophoretograms of CD44-shRNA identified by PCR. Lanes 1 and 3: negative clone; Lanes 2 and 4–8: positive clone; Lane M: DNA marker (the standard bands were 2000 bp, 1000 bp, 750 bp, 500 bp, 250 bp, and 100 bp in succession from the up to the bottom. (b) CD44-shRNA sequencing comparison results. The sequencing comparison confirmed there are correct clones indicating successful construction of the CD44-v6-shRNA plasmid.

a stable and efficient gene carrier system is one of the most vital factors for gene therapy [14, 15]. Many studies on the function of magnetic nanocarriers are available. It is reported that adriamycin uptake by glioma cell can be enhanced by using magnetic NPs as the carriers [16]. Fe_3O_4 NPs modified by sodium alginate and D-galactosamine (Fe_3O_4 @Alg-GA NPs) can enhance the uptake by human hepatoma cells and produce the heating effect under action of alternating magnetic field [17].

A pancreatic cancer research shows that the chemotherapeutic adriamycin could be effectively transported and released in cancer cells by using superparamagnetic iron oxide NPs as carriers [18]. More inspiringly, a new administration route is discovered in brain tumor animal experiments. DL-lactic acid-glycolic acid (PLGA) magnetic NPs were employed for the targeted therapy (using paclitaxel (PTX) and curcumin) for glioma mouse. As a result, chemotherapeutics can rapidly pass the blood brain barrier

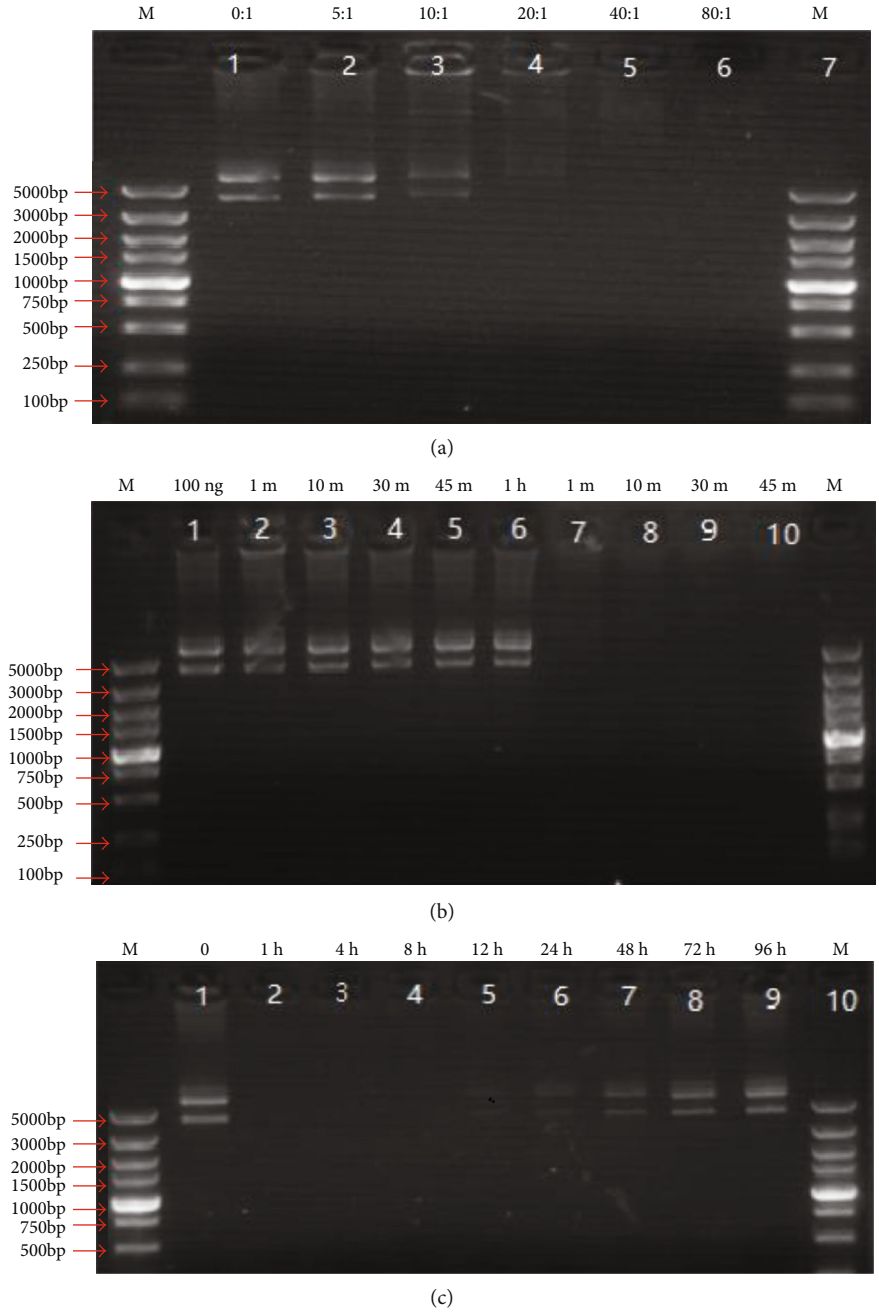

Figure 6: Binding, digestion, and release of PEG-MZF-NPs with CD44-shRNA. (a) Electrophoretograms of PEG-MZF-NPs with various mass ratios after binding with CD44-shRNA plasmids. Lane 1—0 : 1 (100 ng plasmid DNA, with no PEG-MZF-NPs); Lane 2—5 : 1; Lane 3—10 : 1; Lane 4—20 : 1; Lane 5—40 : 1; Lane 6—80 : 1. The electrophoresis images of binding, release, and digestion protection experiments suggested that when plasmid was added at the ratios of 0 : 1, 5 : 1, 10 : 1, 20 : 1, and 40 : 1, clear bands could be seen in lanes. When the mass ratio of magnetic NPs to CD44-shRNA was 40 : 1, the former could practically bind with all plasmids in the system indicating 40 : 1 was an optimal binding ratio. (b) Electrophoretograms of the release experiment of PEG-MZF-NP-CD44-shRNA plasmid complex. Lane 1: 100 ng original plasmid DNA; Lane 2: 1 h; Lane 3: 4 h; Lane 4: 8 h; Lane 5: 12 h; Lane 6: 24 h; Lane 7: 48 h; Lane 8: 72 h; Lane 8: 96 h. Within 1, 4, 8, 12, and 24 h and 2 days, DNA was released at a large amount, but in between day 3 and day 4 it was not greatly different and PEG-MZF-NPs could protect plasmid and effectively release DNA. (c) Digestion protection experiment of PEG-MZF-NPs-CD44-shRNA plasmid complex. Lane 1: 100 ng original plasmid DNA; Lane 2: complex for 1 min; Lane 3: complex for 10 min; Lane 4: complex for 30 min; Lane 5: complex for 45 min; Lane 6: complex for 1 h. In the stability research, the DNase-I digestion experiment was used to observe stability of magnetic nanomaterial/gene complex. The band lightness of PEG-MZF-NP/CD44-shRNA complex in electrophoresis image showed no obvious changes within the first 60 min demonstrating its stability. The exposed CD44-shRNA plasmids were almost digested by DNase-I within 1 min suggesting a good stability of complex, and PEG-MZF-NPs could protect CD44-shRNA from nuclease digestion (Figure 6(c)).

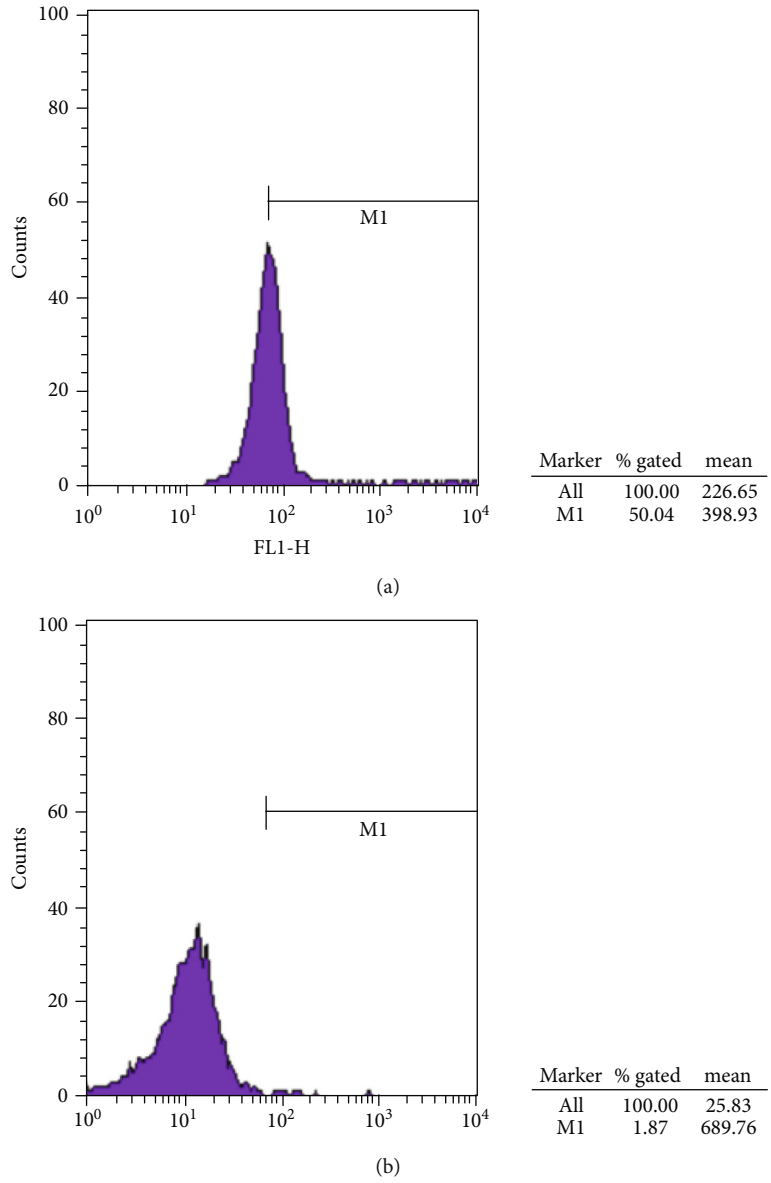

Figure 7: The transfection efficiency comparison of PEG-MZF-NPs and liposome ((a) PEG-MZF-NP group, (b) liposome group). PEG-MZF-NPs as carriers to transfect CD44-shRNA-EGFP plasmids into the ovarian cancer cells, and transfection efficiency is ((a) 58.87 ± 3.21%) analyzed by flow cytometry which is higher than in the liposome transfection method ((b) 50.04 ± 3.02%).

(BBB) depending on carriers [19]. This finding provides a new idea to solve the problem that many chemotherapeutics cannot pass BBB. A favorable efficacy was accomplished in a research on the combination of magnetic fluid hyperthermia with As_2O_3 chemotherapy to treat hepatoma using $Mn_{0.5}Zn_{0.5}Fe_2O_4$-NPs as a carrier which has homoeothermic and automatic temperature control properties [20]. In the present study, biological characteristic detection indicated that PEG-MZF-NPs can bind with CD44-shRNA plasmids and protect the DNA from nuclease digestion. In appropriate conditions, DNA can effectively release from the complex. These findings demonstrate a good potential to serve as a gene-transferring carrier. We used PEG-MZF-NPs as carriers to transfect CD44-shRNA-EGFP plasmids into ovarian cancer cells, and the transfection efficiency is 58.87 ± 3.21% as analyzed by flow cytometry (Figure 7(a)), higher than 50.04 ± 3.02% of the liposome transfection method (Figure 7(b)) confirming feasibility of PEG-MZF-NPs serving as the gene transfer carriers in gene therapy.

Up to now, many gene therapies have been used in research on multiple tumor treatment. Among them, RNAi technology has displayed a promising application prospect. In research on multiple myeloma, RNAi technology was employed to silence PSMD10 gene expression and showed good results [21]. Suppressing PRDM14 expression by RNAi technology can reduce the size and metastasis of breast cancer [22]. In addition, RNAi technology can also be used to specifically suppress the expression of oncogene and cancer-related gene which can thereby render these genes at

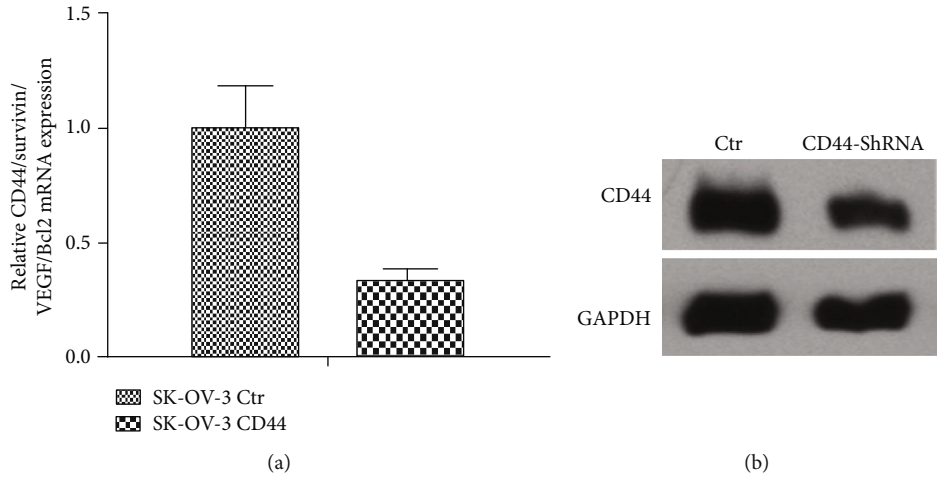

Figure 8: CD44 mRNA and protein expression in SK-OV-3 cells. (a) CD44 mRNA expression in ovarian cancer SK-OV-3 cells transfected with CD44-shRNA plasmid. CD44 protein expression in ovarian cancer SK-OV-3 cells transfected with CD44-shRNA plasmids. Using PEG-MZF-NPs as carriers, CD44-shRNA plasmids and the empty plasmids were transfected into ovarian cancer SK-OV-3 cells. (b) Western blotting results suggested that protein expression in the transfected cells is markedly downregulated.

a silence state thus displaying favorable effects in antitumor treatment. Besides, it is discovered that inhibiting FKBP14 expression through RNAi technology can lower the proliferation capacity of ovarian cancer cells [23]. Restraining CD44 gene expression could markedly inhibit the growth of ovarian cancer cells, suppress tumor angiogenesis, and reduce tumor recurrence and metastasis [24]. Typically, ovarian cancer patients with high CD44 expression showed high chemoresistance [25]. Additionally, CD44 knockout ovarian cancer mice had markedly lowered cell proliferation, migration, and invasion capacities, but with enhanced drug sensitivity [26]. Suppressing CD44 gene by siRNA can promote the chemosensitivity of ovarian cancer cells to PTX thus inhibiting tumor cell growth [27]. Thus, it can be figured out that CD44 may become a new promising target in ovarian cancer treatment. As usual, RNA or DNA was constructed and assembled into magnetic nanoparticles by electrostatic, hydrophobic interaction and loading methods so as to transfect or deliver RNA or DNA. In this study, the CD44-shRNA plasmids have been constructed and transfected into ovarian cancer HO8910 cells with PEG-MZF-NPs as carriers. RT-PCR and Western blotting results suggested that CD44 mRNA and protein expression in transfected cells is markedly downregulated (Figure 8). These findings further verify the successful construction of CD44-shRNA plasmid as well as its feasibility of treating PEG-MZF-NPs as the gene transfer carriers in tumor gene therapy which can provide a new idea and method for comprehensive treatment of ovarian cancer in clinic.

4. Conclusions

We successfully prepared PEG-MZF-NPs with favorable dispersity, magnetic responsiveness, and BC. Typically, the excellent magnetothermal effect can be used for tumor magnetothermal therapy. *In vitro* MRI showed a good application potential for being magnetic resonance T2 relaxation contrast agents and the possibility to realize an integration of targeting diagnosis and treatment. The CD44-shRNA plasmids have been successfully constructed, and PEG-MZF-NPs may serve as the carriers for gene therapy. The pegylated magnetic manganese zinc ferrite nanoparticles have favorable magnetic responsiveness, biocompatibility, and a magnetothermal effect as well as good gene transfection efficiency. They are potential candidates to serve as carriers in gene therapy and to serve as magnetothermal mediators for tumor magnetic hyperthermia.

Data Availability

The graphics and quantitative data used to support the findings of this study are included within the article.

Conflicts of Interest

The authors declare that they have no conflicts of interest.

Authors' Contributions

Ting Guo and Fengxiao Dou contributed equally to this work.

Acknowledgments

This work was financially supported by the National Natural Science Foundation of China (81571797), Natural Science Foundation of Jiangsu, China (BK20151352), Taizhou People's Hospital Medical Innovation Team Foundation, China (CXTDA201901), and Scientific Research Foundation of Taizhou People's Hospital (ZL201734/ZL201717), China.

References

[1] B. K. Lim, E. C. Tighe, and S. D. Kong, "The use of magnetic targeting for drug delivery into cardiac myocytes," *Journal of Magnetism and Magnetic Materials*, vol. 473, pp. 21–25, 2019.

[2] J. N. Jones Buie, Y. Zhou, A. J. Goodwin et al., "Application of deacetylated poly-N-acetyl glucosamine nanoparticles for the delivery of miR-126 for the treatment of cecal ligation and puncture-induced sepsis," *Inflammation*, vol. 42, no. 1, pp. 170–184, 2019.

[3] R. Megías, M. Arco, J. Ciriza et al., "Design and characterization of a magnetite/PEI multifunctional nanohybrid as non-viral vector and cell isolation system," *International Journal of Pharmaceutics*, vol. 518, no. 1-2, pp. 270–280, 2017.

[4] M. Lin, J. X. Huang, X. Jiang et al., "A combination hepatoma-targeted therapy based on nanotechnology: pHRE-Egr1-HSV-TK/^{131}I-antiAFPMcAb-GCV/MFH," *Scientific Reports*, vol. 6, 2016.

[5] T. Guo, M. Lin, J. Huang et al., "The recent advances of magnetic nanoparticles in Medicine," *Journal of Nanomaterials*, vol. 2018, Article ID 7805147, 8 pages, 2018.

[6] M. Lin, J. Huang, J. Zhang et al., "The therapeutic effect of PEI-Mn0.5Zn0.5Fe2O4nanoparticles/pEgr1-HSV-TK/GCV associated with radiation and magnet-induced heating on hepatoma," *Nanoscale*, vol. 5, no. 3, pp. 991–1000, 2013.

[7] J. Xie, C. Yan, Y. Zhang, and N. Gu, "Shape evolution of "multibranched" Mn–Zn Ferrite nanostructures with high performance: a transformation of nanocrystals into nanoclusters," *Chemistry of Materials*, vol. 25, no. 18, pp. 3702–3709, 2013.

[8] Y. Panahi, M. Farshbaf, M. Mohammadhosseini et al., "Recent advances on liposomal nanoparticles: synthesis, characterization and biomedical applications," *Artificial Cells Nanomedicine and Biotechnology*, vol. 45, no. 4, pp. 788–799, 2017.

[9] B. Rathore, K. Sunwoo, P. Jangili et al., "Nanomaterial designing strategies related to cell lysosome and their biomedical applications: a review," *Biomaterials*, vol. 211, pp. 25–47, 2019.

[10] M. Lin, J. Huang, and M. Sha, "Recent advances in nanosized Mn-Zn ferrite magnetic fluid hyperthermia for cancer treatment," *Journal of Nanoscience and Nanotechnology*, vol. 14, no. 1, pp. 792–802, 2014.

[11] E. Khodaverdi, Z. Tayarani-Najaran, E. Minbashi et al., "Docetaxel-loaded mixed micelles and polymersomes composed of poly (caprolactone)-poly (ethylene glycol) (PEG-PCL) and poly (lactic acid)-poly (ethylene glycol) (PEG-PLA): preparation and in-vitro characterization," *Iranian Journal of Pharmaceutical Research*, vol. 18, no. 1, pp. 142–155, 2019.

[12] A. S. Ahmed and R. V. Ramanujan, "Curie temperature controlled self-healing magnet–polymer composites," *Journal of Materials Research*, vol. 30, no. 7, pp. 946–958, 2015.

[13] S. Faraji, G. Dini, and M. Zahraei, "Polyethylene glycol-coated manganese-ferrite nanoparticles as contrast agents for magnetic resonance imaging," *Journal of Magnetism and Magnetic Materials*, vol. 475, pp. 137–145, 2019.

[14] M. K. Riley II and W. Vermerris, "Recent advances in nanomaterials for gene delivery-a review," *Nanomaterials*, vol. 7, no. 5, p. 94, 2017.

[15] L. Naldini, "Gene therapy returns to centre stage," *Nature*, vol. 526, no. 7573, pp. 351–360, 2015.

[16] I. Venugopal, S. Pernal, A. Duproz, J. Bentley, H. Engelhard, and A. Linninger, "Magnetic field-enhanced cellular uptake of doxorubicin loaded magnetic nanoparticles for tumor treatment," *Materials Research Express*, vol. 3, no. 9, 2016.

[17] Y. Yamamoto, T. Itoh, and T. Irieda, "A heat dissipation study of iron oxide nanoparticles embedded an agar phantom for the purpose of magnetic fluid hyperthermia," *Journal of Nanoscience and Nanotechnology*, vol. 19, no. 9, pp. 5469–5475, 2019.

[18] M. P. Arachchige, S. S. Laha, A. R. Naik, K. T. Lewis, R. Naik, and B. P. Jena, "Functionalized nanoparticles enable tracking the rapid entry and release of doxorubicin in human pancreatic cancer cells," *Micron*, vol. 92, pp. 25–31, 2017.

[19] Y. Cui, M. Zhang, F. Zeng, H. Jin, Q. Xu, and Y. Huang, "Dual-targeting magnetic PLGA nanoparticles for codelivery of paclitaxel and curcumin for brain tumor therapy," *ACS Applied Materials & Interfaces*, vol. 8, no. 47, pp. 32159–32169, 2016.

[20] L. Wang, J. Zhang, Y. An et al., "A study on the thermochemotherapy effect of nanosized As2O3/MZF thermosensitive magnetoliposomes on experimental hepatomain vitroandin vivo," *Nanotechnology*, vol. 22, no. 31, p. 315102, 2011.

[21] S. Du, W. Qin, H. Leng, Z. Chen, and T. Zhang, "Construction of a recombinant lentivirus-mediated shRNA expression vector targeting the human PSMD10 gene and validation of RNAi efficiency in RPMI-8226 multiple myeloma cells," *Oncology Reports*, vol. 38, no. 2, pp. 809–818, 2017.

[22] H. Taniguchi, D. Hoshino, C. Moriya et al., "Silencing PRDM14 expression by an innovative RNAi therapy inhibits stemness, tumorigenicity, and metastasis of breast cancer," *Oncotarget*, vol. 8, no. 29, pp. 46856–46874, 2017.

[23] M. Lu, Y. Miao, L. Qi, M. Bai, J. Zhang, and Y. Feng, "RNAi-mediated downregulation of fkbp14 suppresses the growth of human ovarian cancer cells," *Oncology Research*, vol. 23, no. 6, pp. 267–274, 2016.

[24] L. Zou, T. Yi, X. Song, S. Li, Y. Wei, and X. Zhao, "Efficient inhibition of intraperitoneal human ovarian cancer growth by short hairpin RNA targeting CD44," *Neoplasma*, vol. 61, no. 3, pp. 274–282, 2014.

[25] L. Zhao, C. Gu, K. Huang et al., "The prognostic value and clinicopathological significance of CD44 expression in ovarian cancer: a meta-analysis," *Archives of Gynecology and Obstetrics*, vol. 294, no. 5, pp. 1019–1029, 2016.

[26] C. Chen, S. Zhao, A. Karnad, and J. W. Freeman, "The biology and role of CD44 in cancer progression: therapeutic implications," *Journal of Hematology & Oncology*, vol. 11, no. 1, 2018.

[27] R. Edelman, Y. G. Assaraf, A. Slavkin, T. Dolev, T. Shahar, and Y. D. Livney, "Developing body-components-based theranostic nanoparticles for targeting ovarian cancer," *Pharmaceutics*, vol. 11, no. 5, p. 216, 2019.